NASA MEMO 2-28-59L

NASA

MEMORANDUM

COMPARISON OF MEASURED FLAPWISE STRUCTURAL BENDING MOMENTS ON A TEETERING ROTOR BLADE WITH RESULTS CALCULATED FROM THE MEASURED PRESSURE DISTRIBUTION

By Alton P. Mayo

Langley Research Center
Langley Field, Va.

NATIONAL AERONAUTICS AND SPACE ADMINISTRATION

WASHINGTON
March 1959

NATIONAL AERONAUTICS AND SPACE ADMINISTRATION

MEMORANDUM 2-28-59L

COMPARISON OF MEASURED FLAPWISE STRUCTURAL BENDING MOMENTS ON A TEETERING ROTOR BLADE WITH RESULTS CALCULATED FROM THE MEASURED PRESSURE DISTRIBUTION

By Alton P. Mayo

SUMMARY

Flapwise bending moments were calculated for a teetering rotor blade using a reasonably rapid theoretical method in which airloads obtained from wind-tunnel tests were employed. The calculated moments agreed reasonably well with those measured with strain gages under the same test conditions. The range of the tests included one hovering and two forward-flight conditions. The rotor speed for the test was very near blade resonance, and difficult-to-calculate resonance effects apparently were responsible for the largest differences between the calculated and measured harmonic components of blade bending moments. These differences, moreover, were largely nullified when the harmonic components were combined to give a comparison of the calculated and measured blade total-moment time histories.

The degree of agreement shown is therefore considered adequate to warrant the use of the theoretical method in establishing and applying methods of prediction of rotor-blade fatigue loads. At the same time, the validity of the experimental methods of obtaining both airload and blade stress measurement is also indicated to be adequate for use in establishing improved methods for prediction of rotor-blade fatigue loads during the design stage.

The blade stiffnesses and natural frequencies were measured and found to be in close agreement with calculated values; however, for a condition of blade resonance the use of the experimental stiffness values resulted in better agreement between calculated and measured blade stresses.

INTRODUCTION

The ultimate goal of being able to predict theoretically helicopter rotor-blade stresses for design purposes requires that the validity of the theoretical methods be established by comparison with experimental measurements. In the past, extensive amounts of bending-moment data have been measured with strain gages on helicopter blades. Recently, the airloads have also been measured on a blade through the use of electrical pressure cells. However, a demonstration of the validity of a reasonably expeditious theoretical method for correlating these two types of measurements has been lacking.

In this investigation the accuracy of a relatively rapid theoretical method for computing stresses from airloads is demonstrated by using some experimental load and moment measurements. The airloads and structural moments measured on a teetering helicopter blade in the Langley full-scale tunnel are presented along with the calculated blade structural moments obtained by using the measured airloads and the theoretical methods of reference 1. The comparisons are shown for one hovering condition and for two forward-flight speeds. Also shown are some comparisons between the experimental and calculated blade stiffness and natural frequencies.

SYMBOLS

C_T	thrust coefficient, $\frac{T}{\pi R^2 \rho (\Omega R)^2}$
EI	blade bending stiffness, lb-in.^{2}
g	structural damping coefficient
l	blade section loading, lb/in.
l_o	blade section steady loading, lb/in.
M	blade bending moment, lb-in.
M_o	blade steady bending moment, lb-in.
N	harmonic number
r	radial distance to blade element from rotor shaft axis, in.

T	rotor thrust, lb
R	radial distance from rotor shaft axis to blade tip, in.
V	forward velocity, in./sec
z	blade deflection, positive upward, in.
α	rotor angle of attack; angle between axis of no feathering and line perpendicular to flight path, positive rearward, deg
μ	tip-speed ratio, $\frac{V \cos \alpha}{\Omega R}$
ρ	mass density of air, $\frac{\text{lb-sec}^2}{\text{in.}^4}$
ψ'	blade azimuth angle for pressure coefficients when uncorrected for instrument lag; measured from downwind position in direction of rotation, deg
ψ	blade azimuth angle measured from downwind position in direction of rotation, deg
ω	angular frequency of harmonic loading, radians/sec
Ω	rotor angular velocity, radians/sec

Subscripts:

1,2,. . .N	harmonic number
C	cosine component
S	sine component

APPARATUS AND TEST

In the investigation the airloads and the flapwise bending moments were measured on a teetering rotor blade for one hovering and two forward-flight conditions in the Langley full-scale tunnel. A general view of the model mounted for tests in the Langley full-scale tunnel is shown in figure 1. The hovering measurements were made at $C_T = 0.0049$

and $\Omega R = 497$ feet per second. The forward-flight measurements were made at tip-speed ratios of 0.076 and 0.15 for thrust coefficients of approximately 0.004 and 0.005, respectively. In order to determine some of the blade structural characteristics, measurements were also made of the blade stiffness, natural frequencies, and structural damping.

Blade Characteristics

The rotor blade had an NACA 0012 airfoil section, was rectangular in plan form, had no twist, had a radius of 91.5 inches, and had a 14-inch chord. The forward portion of the blade, from the leading edge to the quarter chord, was formed of an aluminum D-section spar covered with balsa fairing strips. The rear portion was built up of plywood ribs and balsa planking and then the entire blade was covered with one layer of fiber glass impregnated with Paraplex resin. This type of construction resulted in a very rigid airfoil section. Some further details are given in figure 2 and in references 2 and 3. Reference 3 also describes the hub in greater detail.

In order to obtain an experimental estimate of the blade flapwise bending stiffness, a 50-pound weight was applied to the blade near the tip and the deflections were measured at several spanwise stations with dial gages. From these measurements a four-term power series for the $1/EI$ distribution was determined. Inversion of the $1/EI$ distribution yielded the experimental EI distribution which is shown in figure 3 along with a theoretically calculated stiffness distribution determined from the structural geometry and the material properties of the sections. The difference between the calculated and experimental stiffness near the blade tip is attributed to the difficulty in obtaining reliable deflection measurements in this region where the applied moment and blade curvature were small. Also shown in figure 3 is the blade weight distribution calculated from the design data on the blade structure and its contents.

The measured blade deflections due to the 50-pound tip load are compared in figure 4 with the calculated blade deflections obtained for the same tip loading by means of equation (10) of reference 1. It can be seen in the figure that the measured blade deflections are 6 percent less than the calculated values. This indicates that the actual blade is stiffer than the theory predicts.

The first symmetric and the first unsymmetric natural frequencies on the nonrotating blade were obtained using a mechanical shaker. The first symmetric natural frequency of the blade was determined to be 7.5 cycles per second and the first unsymmetric frequency, as 19.5 cycles per second. The blade first symmetrical and first unsymmetrical natural frequencies were also calculated using the method outlined in reference 1.

The rotating and nonrotating first-symmetrical-mode natural frequencies were obtained from equations (10) and (18) of reference 1 as applied to the cantilever blade and by using the iteration procedures of reference 4. The rotating first-unsymmetrical-mode natural frequency was obtained from equations (10) and (12) of reference 1 and by employing the aforementioned iteration procedures. These calculated and measured natural frequencies are shown in figure 5 along with a variation of the natural frequencies with rotor speed. This variation was calculated by the method of reference 5 in which the nonrotating natural frequencies and linear approximations to the blade bending stiffness are used.

It can be seen in figure 5 that the calculated and measured natural frequencies are in good agreement. Shown also in this figure is the third harmonic of blade rotational frequency to illustrate that a condition of blade resonance exists around 630 revolutions per minute, which was approximately the rotor speed for the test.

A measure of the blade structural damping coefficient was obtained by plucking the end of the blade, measuring the deflection decay rate, and applying the methods of reference 6. The value of the damping coefficient g obtained was 0.04. The frequency for which this coefficient applies was approximately 8 cycles per second.

Airload Measurements

The airloads were measured using NACA miniature electrical pressure gages. Fifty pressure gages mounted inside the blade measured the chordwise load distribution at five spanwise stations. (See fig. 2.) The measurements were transmitted from the rotor through slip rings and recorded on an oscillograph. Further details of the pressure-cell installation are given in reference 2.

Strain-Gage Measurements

In the strain-gage test, the blade structural moments were measured with gages mounted on the fiber glass covering at the five spanwise stations shown in figure 2. The strain gages were calibrated for bending loads only and the application of a constant load at various chordwise stations showed that these gages did not respond to torsion. The effect of centrifugal tension loads on the strain-gage response under test conditions was minimized by taking a zero reading before each run with the blade rotating at zero thrust. The moment measurements were transmitted from the rotor through slip rings and recorded on an oscillograph. Because of the limited number of slip rings and the limited instrumentation space on the hub, the airloads and structural moments could not be measured simultaneously. The strain-gage data were, therefore, obtained

in reruns of the pressure-distribution test. In these reruns the conditions were duplicated as closely as possible.

REDUCTION OF DATA

Because the theoretical methods used to calculate the structural moments from the measured airloads were applicable only to a load and a moment component of a single frequency, the measured airload and bending-moment data were reduced by Fourier methods to obtain the harmonic components - each of a frequency that was an integer multiple of the blade rotational frequency.

The oscillograph trace for each strain gage was read at 48 points per revolution for 10 revolutions. The readings were then averaged and used in Fourier methods to obtain the harmonic components as Fourier coefficients. The general equation to which the Fourier methods were applied was of the form

$$M = M_0 + M_{1C} \cos \psi + M_{1S} \sin \psi + M_{2C} \cos 2\psi + \ldots M_{12S} \sin 12\psi \qquad (1)$$

In the analysis of this paper only the M_0, M_{1C}, M_{1S}, M_{2C}, M_{2S}, M_{3C}, M_{3S}, M_{4C}, and M_{4S} coefficients are considered.

The procedures for the pressure-data reduction were somewhat similar to those used for the strain gages. A complete discription of the reduction of the pressure data is given in reference 3. The subscript symbols used with the letter l denote that the various loading coefficients obtained from the pressure data were identical to those used to denote the moment coefficients just discussed.

The measured airload data of figures 6 to 11 were not corrected for instrumentation lag. The load coefficients which are presented in this paper contain the 8° lag per harmonic described in reference 3 (i.e., 8° for the first harmonic, 16° for the second harmonic, etc.). There was no appreciable lag in the measured moment data.

RESULTS AND DISCUSSION

Comparisons between the calculated and measured structural moments were obtained for one hovering and two forward-flight conditions. The calculated moments were obtained by using the measured airloads and the

theoretical methods of reference 1. For the theoretical comparisons a correction for the measured airload time lag previously mentioned was made. Torsion effects were not included in the calculations since the blade was very rigid in torsion (see ref. 3), and as previously mentioned, torsion loads were shown to have no effect on the bending-moment gages.

Hovering

Measured results.- Time histories of the airloads and structural moments measured in hovering are shown in figure 6. The airloads shown in figure 6 are for a 540-pound thrust, whereas the moment data are for a 490-pound thrust; the 490-pound-thrust airload data were destroyed prior to the preparation of this paper. The airload for a 540-pound-thrust condition indicates the general airload behavior.

As may be seen in figure 6 there were some fairly large variations in the bending moments with azimuth. The reason for these variations is not understood; however, they might be attributed to the fact that the hovering rotor speed (623 rpm) was near blade resonance (fig. 5) and small excitations may have existed because of a nonsymmetrical recirculating flow field and possible blade pitch oscillations due to freedom in the control system. In order to obtain steady values for comparison with calculated results an average was obtained from the measured values.

Calculated results.- The calculated structural moments obtained using the average measured airload and the methods of reference 1 are shown in figure 7 of this paper along with the measured moment values. The blade weight and stiffness used in the calculations was that given in figure 3.

The measured and calculated structural moments which are compared in figure 7 for the hovering condition are in fair agreement. The disagreement shown near the blade tip is suspected to be partially due to measuring error since centrifugal effects are of a relieving nature and the structural moments for the steady conditions are not expected to be equal to nor exceed the aerodynamic moment as is shown in figure 7.

The blade-tip deflection for this hovering condition was calculated by the methods of reference 1 and found to be 1.26 inches measured from the no-load straight-line position. Thus, the 1.26-inch deflection on a 91.5-inch blade reduces the root moment from approximately 15,000 inch-pounds to approximately 8,000 inch-pounds or about 50 percent. This reduction indicates that the centrifugal forces are large and make the blade structural moment very sensitive to blade deflections.

Forward Flight

Airload and structural-moment measurements and some calculated structural moments were obtained for two forward-flight conditions: $\mu = 0.076$, $C_T \approx 0.0039$ and $\mu = 0.15$, $C_T \approx 0.0049$.

Measured results.- Time histories of the airloads and moments measured in forward flight are shown in figures 8 and 9. The curves of the measured loads and moments in forward flight are very nearly the same shape for each revolution of the blade which indicates that there are no sizable load or moment components which have a frequency other than an integer multiple of the rotor rotational frequency. Although there are some fairly large oscillatory airloads measured in forward flight, as may be seen in figures 8 and 9, there are even larger oscillations present in the measured moments. The large difference in the shapes of the load and the moment curves shown in these figures is due mainly to the large amplifications which occurred in the third-harmonic moments because of blade resonance.

Comparison of measured and calculated moments.- Comparisons between the calculated and the experimental structural moments in forward flight are given in figures 10 and 11 for tip-speed ratios of 0.076 and 0.15, respectively. In each figure the harmonic moment components up to the fourth harmonic of the blade rotational frequency are presented.

The calculated moment components for any particular harmonic were obtained by using the measured airloads for that harmonic in the method of reference 1. The blade was treated as a cantilevered blade for the even harmonic loadings, which are symmetrical with respect to the hub, and as a hinged blade for the odd harmonic loadings, which are unsymmetrical with respect to the hub. In the calculations for steady, first, second, and fourth harmonic moment components, the calculated blade weight and stiffness were used and the effects of structural damping were neglected. Because of resonance effects it was decided to include an 0.04 structural damping coefficient in the calculations for the third harmonic and to increase the calculated blade stiffness by 6 percent to be in accord with experimental estimates. This increase in blade stiffness was based on the previously mentioned comparison between the calculated and measured blade deflections (fig. 4) which indicate the blade to be about 6 percent stiffer than the theory had predicted. Calculations were also made for the second-harmonic moments with and without the increased stiffness and the structural damping. There were no appreciable changes in the calculated results.

Steady component.- The measured and calculated structural moments for the forward-flight steady components agreed very well at both forward speeds as may be seen in figures 10(a) and 11(a). This close agreement is probably due to the fact that the steady-load curves are well

defined by the measured data points and that the steady-load blade equations are somewhat simpler than the complete-load blade equations and thus less subject to minor errors.

First-harmonic component.- The measured and calculated moments for the $N = 1$ condition (figs. 10(b) and 11(b)) were in good agreement in some cases and only fair in others. Good agreement was obtained when the measured airload data points formed well-defined load curves. The fairing of the load curves was, for some of the first-harmonic loadings, questionable. The curves were faired to have a reasonable shape and to have a moment of approximately zero at the blade hinge. (A zero aerodynamic moment at the hinge is theoretically expected for the first harmonic of a blade without flapping restraints.) The fairing of the load curves is expected to be one source of error in the calculated moments.

Second-harmonic component.- As may be seen in figures 10(c) and 11(c), the calculated and measured structural moments for the second harmonic agreed fairly well for the outboard stations. The agreement between the measured and calculated root moments, however, was not so good as it was for the outboard station. The reason may be due to small errors in (1) the measured load distribution, (2) the calculated blade stiffness near the root, or (3) the moment measurements.

Third-harmonic component.- The third-harmonic moment components were the most difficult to analyze rigorously. There existed a condition of blade resonance where the physical reaction of the blade is greatly affected by small changes in its mass and stiffness distribution; the blade equations likewise became very sensitive to the same factors. Thus, small errors in the calculated blade weight and stiffness can cause large differences between experimental and calculated results.

The third-harmonic moment components for the $\mu = 0.076$ flight condition, when calculated using the theoretical weight and stiffness and neglecting the effect of structural damping, gave calculated moments twice as large as the measured moments. By arbitrarily including a structural damping coefficient of 0.10 the calculations nearly agreed with the measured moment resultant but not with the proper sine and cosine components. By including a structural damping coefficient of 0.04, as determined from experimental tests, and by increasing the blade stiffness by 6 percent, as indicated by the difference between calculated and measured blade deflections (fig. 4), the calculated moments shown in figure 10(d) for the $\mu = 0.076$ flight condition and in figure 11(d) for the $\mu = 0.15$ flight condition were obtained. As a matter of interest it might be mentioned that a decrease of 6 percent in the assumed blade stiffness gave a calculated flapwise bending moment approximately eight times the measured value for the third harmonic at $\mu = 0.076$.

In figures 10(d) and 11(d) are shown some large differences between the calculated and measured moments even when the theoretical blade stiffness used in the calculations is increased 6 percent to be in accord with the experimental stiffness measurements. Possibly some of the difference in these figures is accounted for in the rotor-speed difference which existed between the load measurements and the moment measurements. The difference in rotor angular velocity between the load and moment measurements was on the order of 2 percent for the $\mu = 0.076$ flight condition and on the order of 4 percent for the $\mu = 0.15$ flight condition. For both flight conditions the blade was operating near a resonant condition as may be seen in figure 5 ($\mu = 0.076$, 623 rpm and $\mu = 0.15$, 600 rpm). Since it is not known how much the airloads near blade resonance were affected by the change in rotor speed and since the calculated results are very dependent, near blade resonance, on the values of blade weight, stiffness, and structural damping, it is believed that further analysis of the differences shown would be dependent on more accurate experimental determination of these quantities.

When the calculated and measured third-harmonic bending moments are compared on a resultant basis rather than on a sine- and cosine-component basis, much of the difference shown is eliminated. Thus, from fatigue-study considerations the differences are ordinarily less significant than those implied by the individual-component comparisons.

Fourth-harmonic component.- The experimental and calculated fourth-harmonic moment components agreed very well as may be seen in figures 10(e) and 11(e). This agreement is rather surprising considering some of the differences obtained for the lower harmonics. Since vertical inertia effects ω^2 are larger than centrifugal effects Ω^2 for the higher harmonics, the agreement at the higher frequencies suggests the possibility of higher accuracy in the vertical inertia terms of the blade equation than in the centrifugal inertia terms.

Calculated blade deflections.- The calculated blade deflections for the first four harmonics are shown in figure 12. These deflections were calculated using equation (10) of reference 1 and the calculated moment values of the previous figures. The required root rotation angle for the first-harmonic deflections was taken from a plot of flapping angle against tip-speed ratio given in reference 3 for the same rotor. At the same tip-speed ratio the loading conditions for the tests of reference 3 and the tests of this investigation were approximately the same. The third-harmonic root angle was obtained from the theoretical calculations. The blade deflections presented in figure 12 give an indication of the relative magnitude of the various harmonic components. Even though the deflections of the higher harmonics are shown to be extremely small as compared with the zero and first-harmonic components, the higher harmonic inertia and aerodynamic damping loads may be fairly large since these loadings vary as ω^2 and $\Omega\omega$, respectively.

Comparison of Total Measured and Calculated Bending Moments

Since the structural soundness and fatigue life of a blade depend on the total structural moment encountered during its operation, it is desirable to know how well the theoretical methods are able to predict the measured moment time histories. Such a comparison between calculated and measured time histories is given in figure 13. In order to obtain figure 13, the calculated moments for the steady and first four harmonics were combined to give a calculated moment time history. The experimental curves shown were likewise obtained from the measured moment coefficients for the steady and first four harmonics. In this manner, the experimental and calculated results are put on the same basis since the effects of the harmonics higher than the fourth are eliminated from both sets of data. Results are shown in figure 13 for three representative spanwise stations for both forward-flight conditions.

As can be seen in figure 13 the measurements and the theory are in good agreement for the $\mu = 0.076$ condition and in fair agreement for the $\mu = 0.15$ condition. Even though some disagreements were observed between the various measured and calculated harmonic moment components for the $\mu = 0.076$ condition, the moment components combined to yield the proper total moments. The agreement between the calculated and measured total moments for $\mu = 0.15$ would probably have been closer if the resonance effects had not occurred in the third-harmonic moment component. The comparisons presented appear to be adequate for fatigue work, especially when it is considered normal practice to avoid near-resonant conditions.

CONCLUDING REMARKS

A reasonably rapid theoretical method was used, in conjunction with measured airloads, to calculate the flapwise bending moments on a teetering helicopter blade. In general, the calculated moment components agreed reasonably well with the experimental measurements; the major differences occurred in the third-harmonic moment components where blade-resonance effects were very large. However, these differences were essentially nullified when the various harmonic moment components were combined to give a comparison of the calculated and measured blade total-moment time histories.

The degree of agreement shown is therefore considered adequate to warrant the use of the theoretical method in establishing and applying methods of prediction of rotor-blade fatigue loads. At the same time, the validity of the experimental methods of obtaining both airload and blade stress measurements is also indicated to be adequate for use in establishing improved methods for prediction of rotor-blade fatigue loads during the design stage.

It was also shown that the calculated blade stiffnesses and natural frequencies were in close agreement with the measured stiffnesses and natural frequencies. However, the calculated blade stiffness was not sufficiently accurate to obtain good third-harmonic moment components where a condition of blade resonance existed. For this condition, the use of the experimental stiffness estimates brought the calculations and the measurements into better agreement.

Langley Research Center,
National Aeronautics and Space Administration,
Langley Field, Va., October 31, 1958.

REFERENCES

1. Mayo, Alton P.: Matrix Method for Obtaining Spanwise Moments and Deflections of Torsionally Rigid Rotor Blades With Arbitrary Loadings. NACA TN 4304, 1958.

2. Rabbott, John P., Jr.: Static-Thrust Measurements of the Aerodynamic Loading on a Helicopter Rotor Blade. NACA TN 3688, 1956.

3. Rabbott, John P., Jr., and Churchill, Gary B.: Experimental Investigation of the Aerodynamic Loading on a Helicopter Rotor Blade in Forward Flight. NACA RM L56I07, 1956.

4. Scanlan, Robert H., and Rosenbaum, Robert: Introduction to the Study of Aircraft Vibration and Flutter. The Macmillan Co., 1951.

5. Yntema, Robert T.: Simplified Procedures and Charts for the Rapid Estimation of Bending Frequencies of Rotating Beams. NACA TN 3459, 1955. (Supersedes NACA RM L54G02.)

6. Gibson, Frederick W.: Determination of the Structural Damping Coefficients of Six Full-Scale Helicopter Rotor Blades of Different Materials and Methods of Construction. NACA TN 3862, 1956.

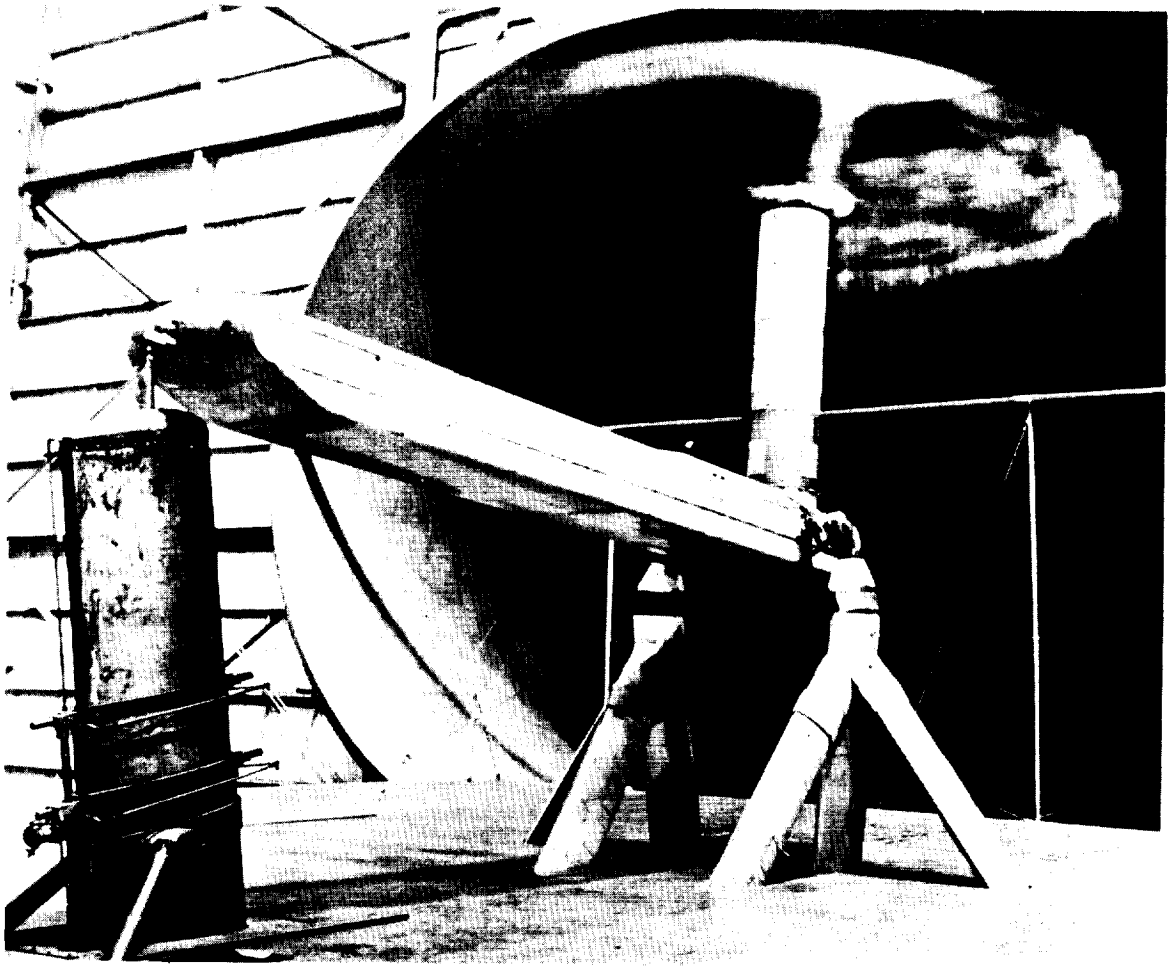

L-83264.2

Figure 1.- General view of model in Langley full-scale tunnel.

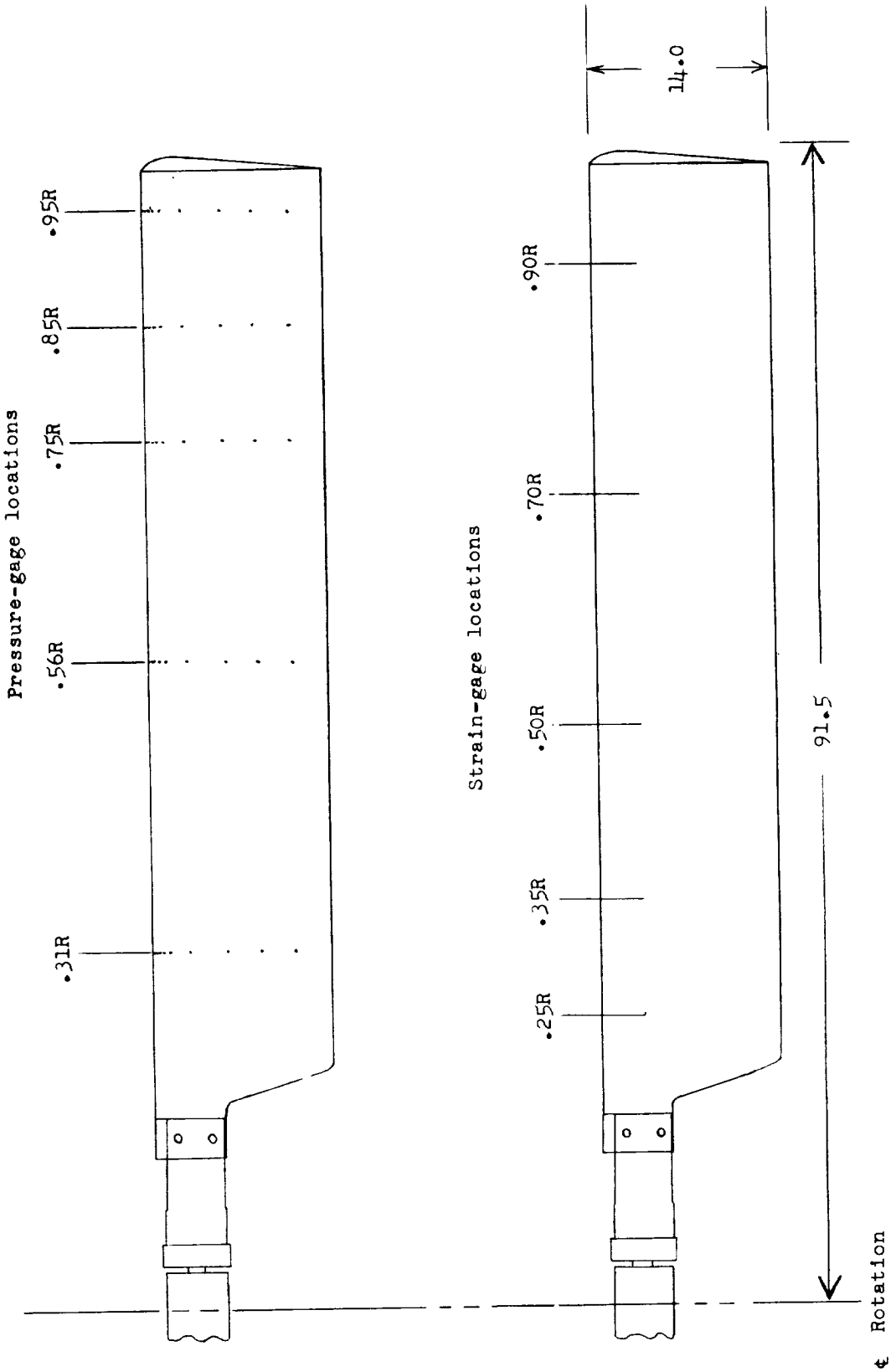

Figure 2.- Blade plan form showing location of pressure gages and strain gages. All dimensions are in inches.

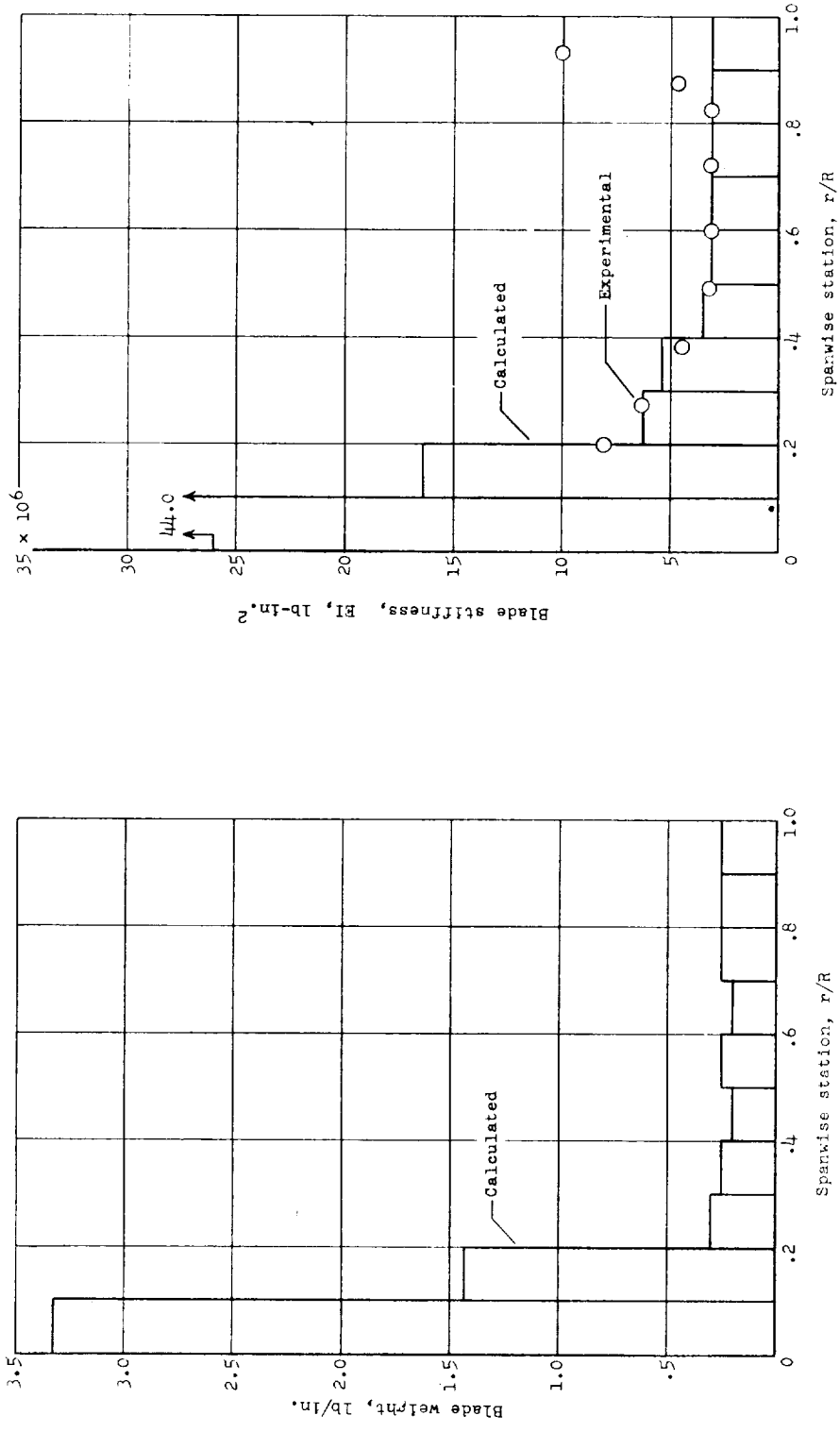

Figure 3.- Blade weight and stiffness distributions.

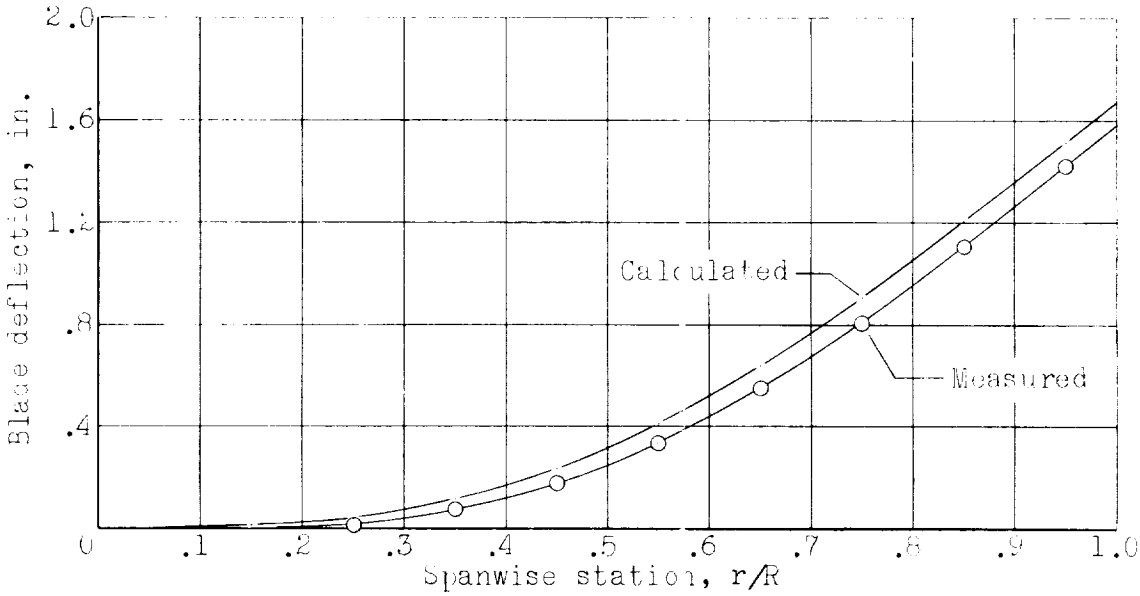

Figure 4.- Comparison of measured and calculated blade deflection due to 50-pound tip load.

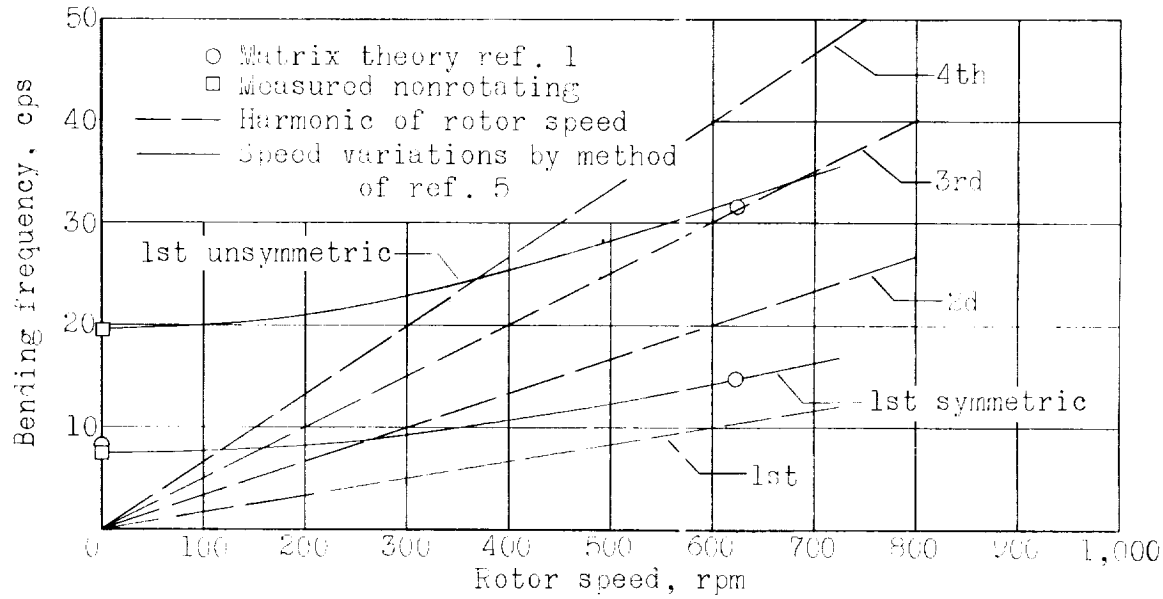

Figure 5.- Comparison of calculated and measured blade-resonance characteristics for various harmonics.

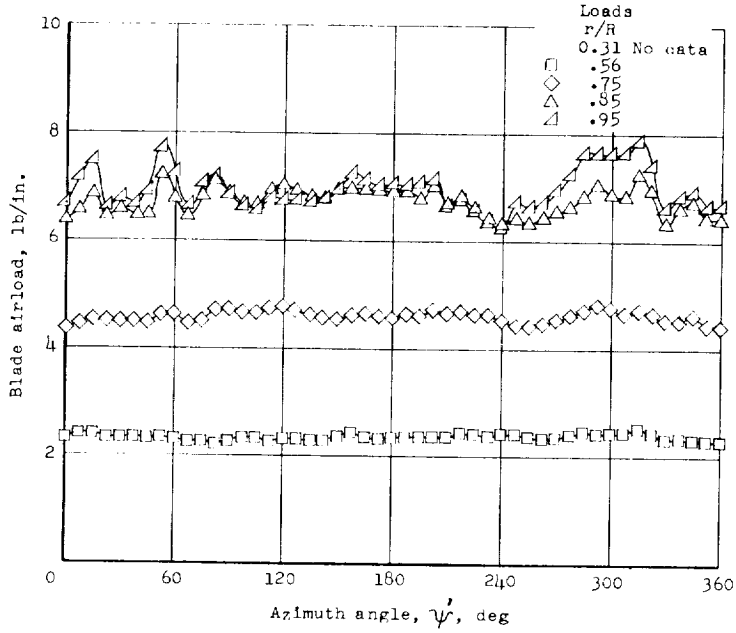

(a) Airloads. Thrust = 540 pounds.

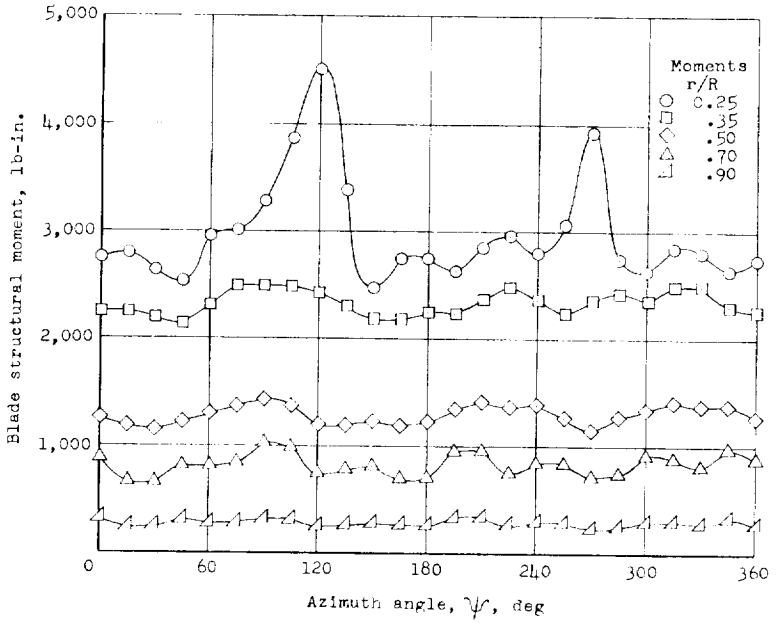

(b) Structural moments. Thrust = 490 pounds.

Figure 6.- Time history of airloads and structural moments measured in hovering condition.

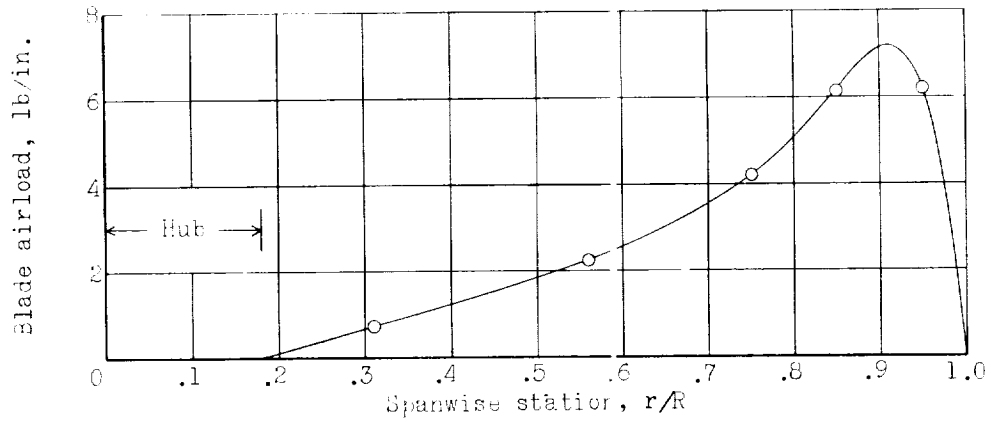

(a) Airloads.

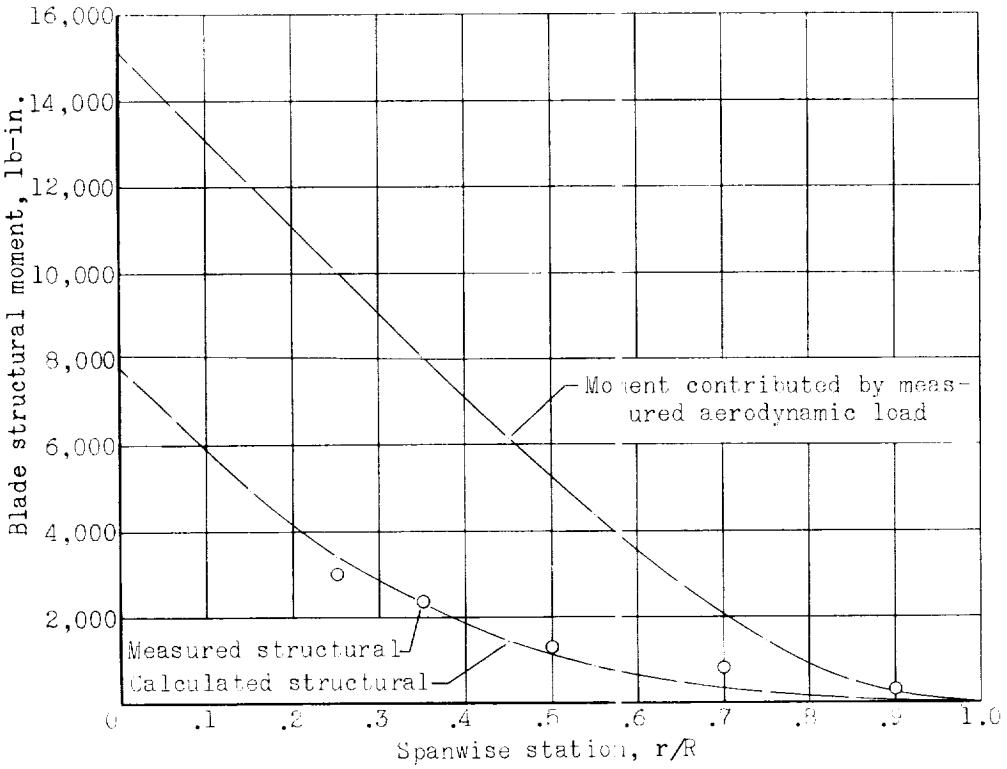

(b) Structural moments.

Figure 7.- Hovering airload and comparison of calculated and measured structural moments in hovering. Thrust = 490 pounds; ΩR = 497 ft/sec; C_T = 0.0049.

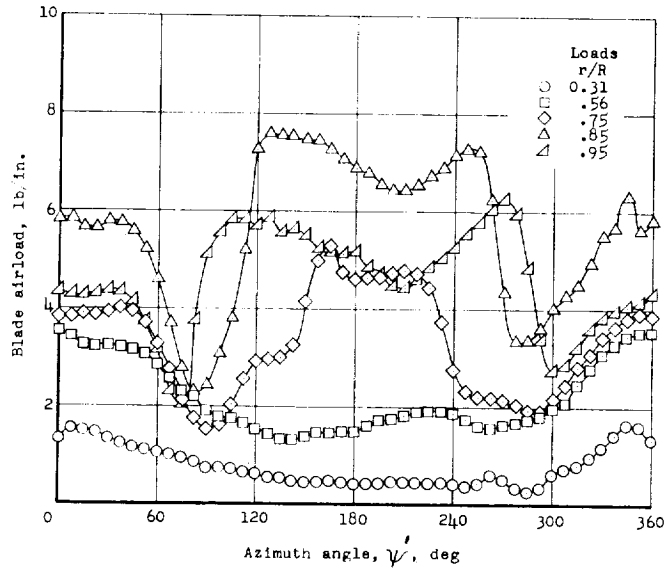

(a) Airloads. $C_T = 0.0041$.

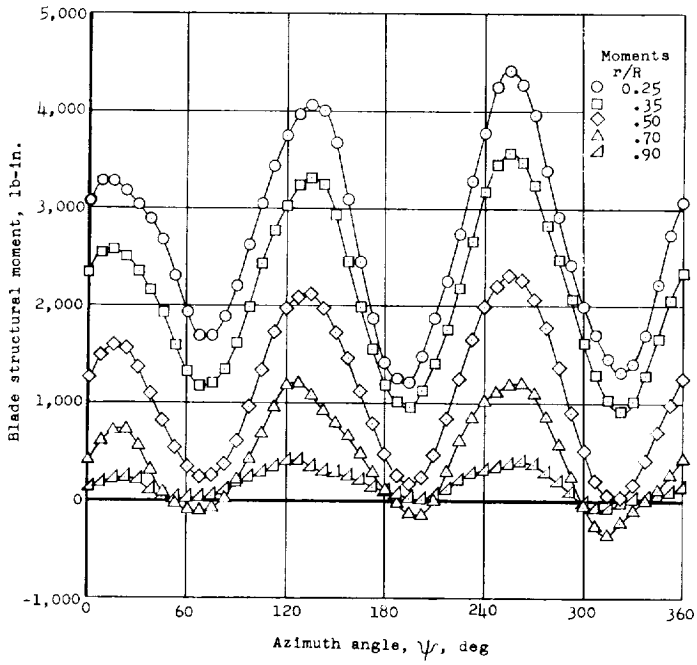

(b) Structural moments. $C_T = 0.0039$.

Figure 8.- Time history of airloads and structural moments measured in forward-flight conditions at $\mu = 0.076$.

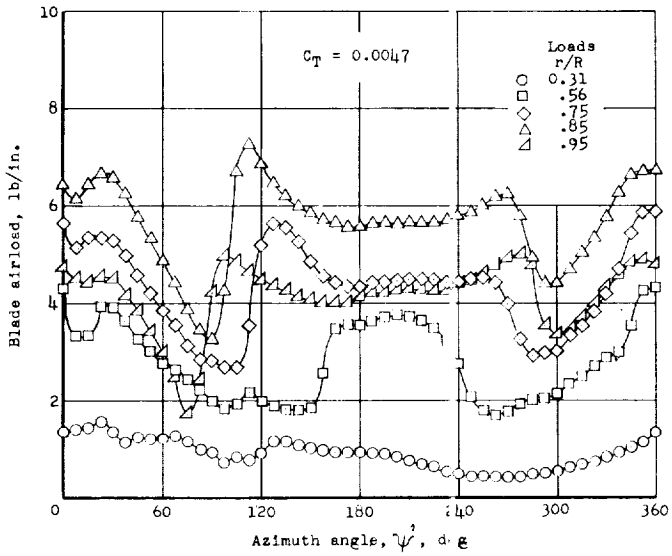

(a) Airloads. C_T = 0.0047.

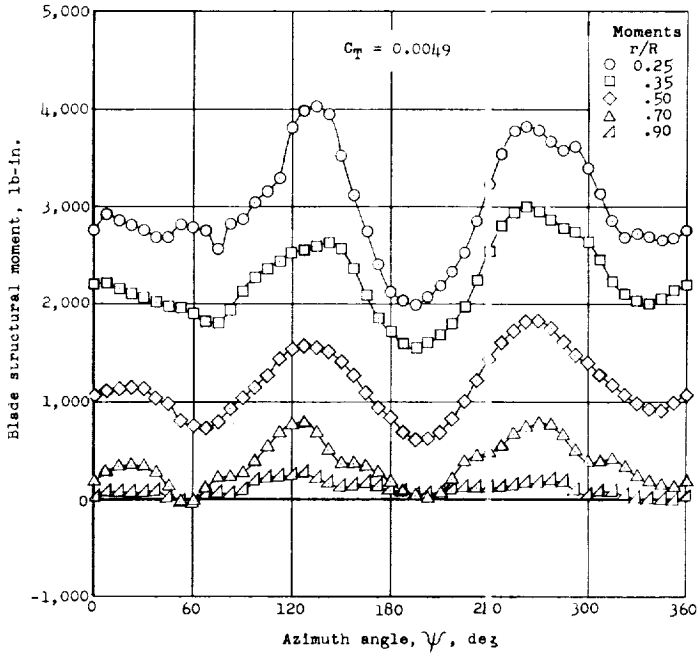

(b) Structural moments. C_T = 0.0049.

Figure 9.- Time history of airloads and structural moments measured in forward-flight conditions at μ = 0.15.

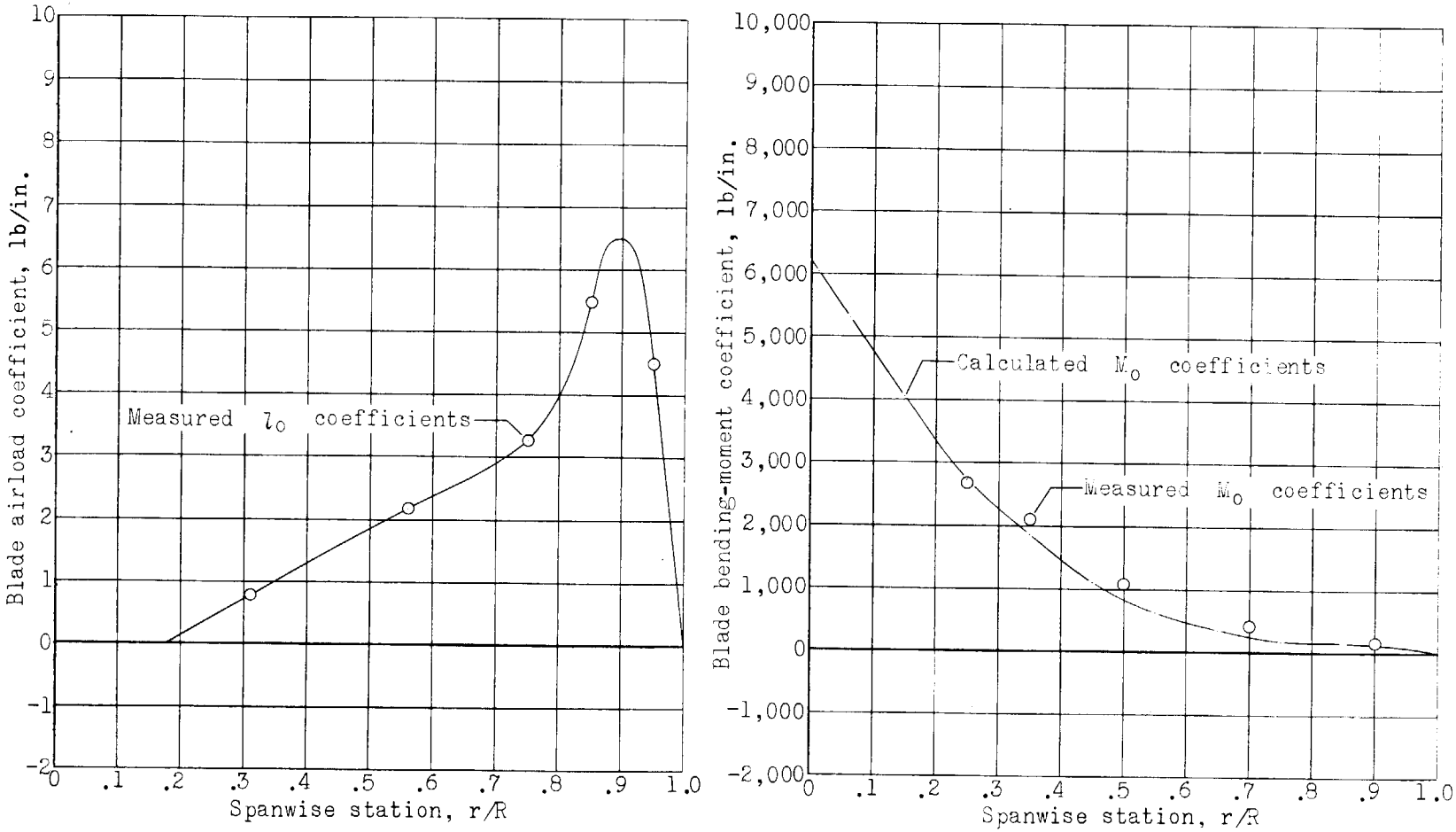

(a) Measured steady airload coefficients and comparison of measured and calculated steady structural moment coefficients.

Figure 10.- Measured airload coefficients and comparison of measured and calculated structural moment coefficients in forward flight. $\mu = 0.076$; airload $C_T = 0.0039$; moment $C_T = 0.0041$.

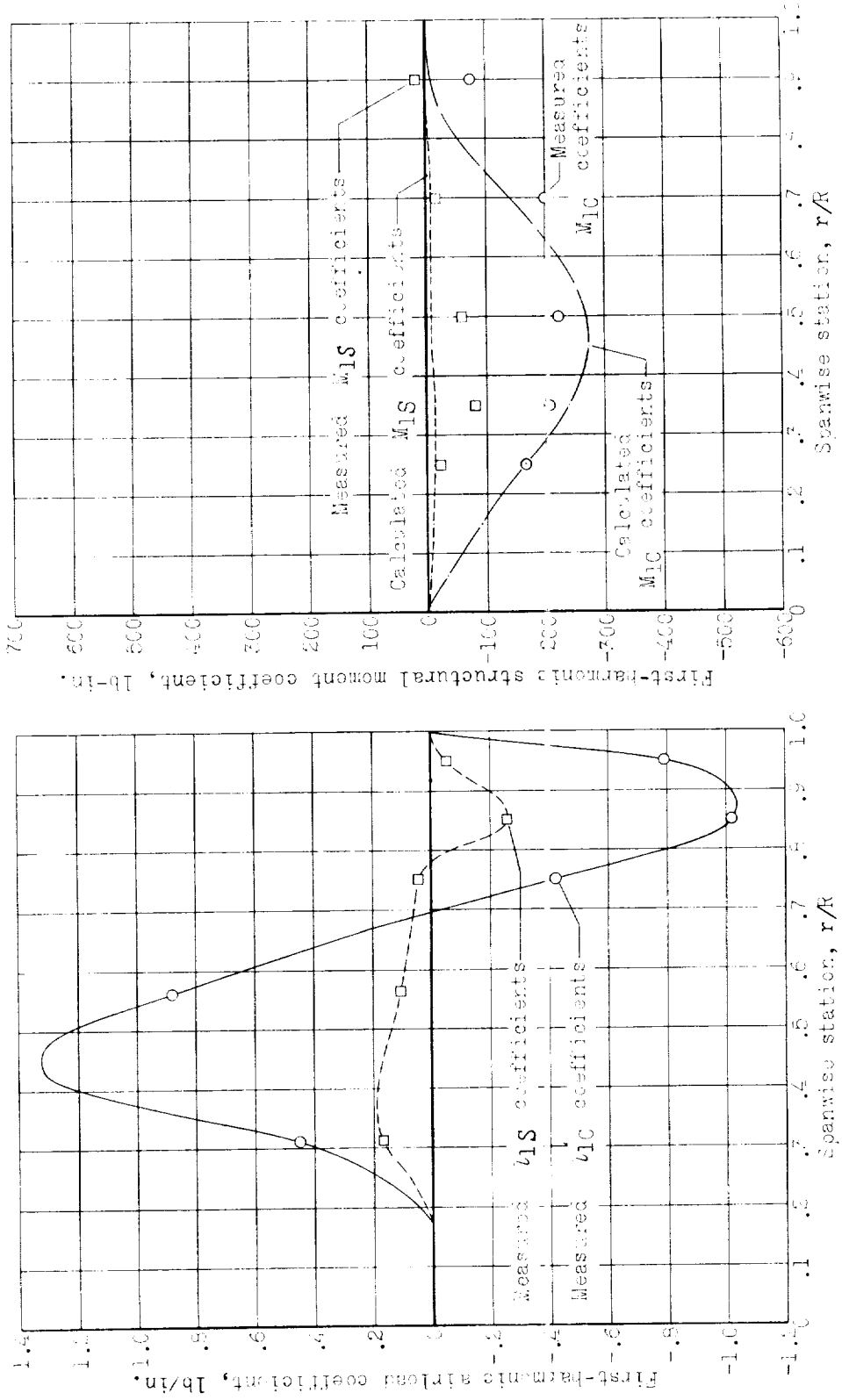

(b) Measured first-harmonic airload coefficients and comparison of measured and calculated first-harmonic structural moment coefficients.

Figure 10.- Continued.

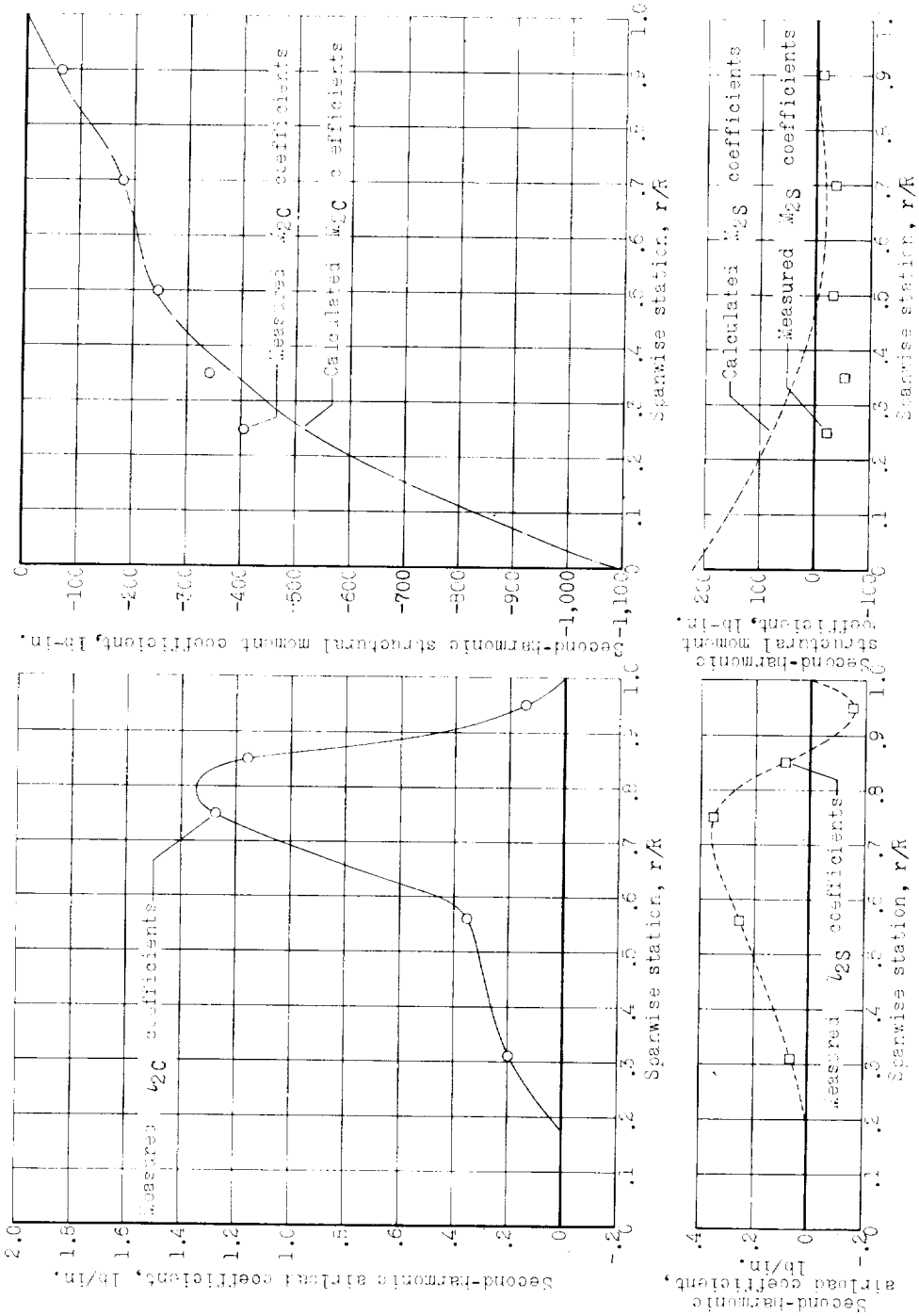

(c) Measured second-harmonic airload coefficients and comparison of measured and calculated second-harmonic structural moment coefficients.

Figure 10.- Continued.

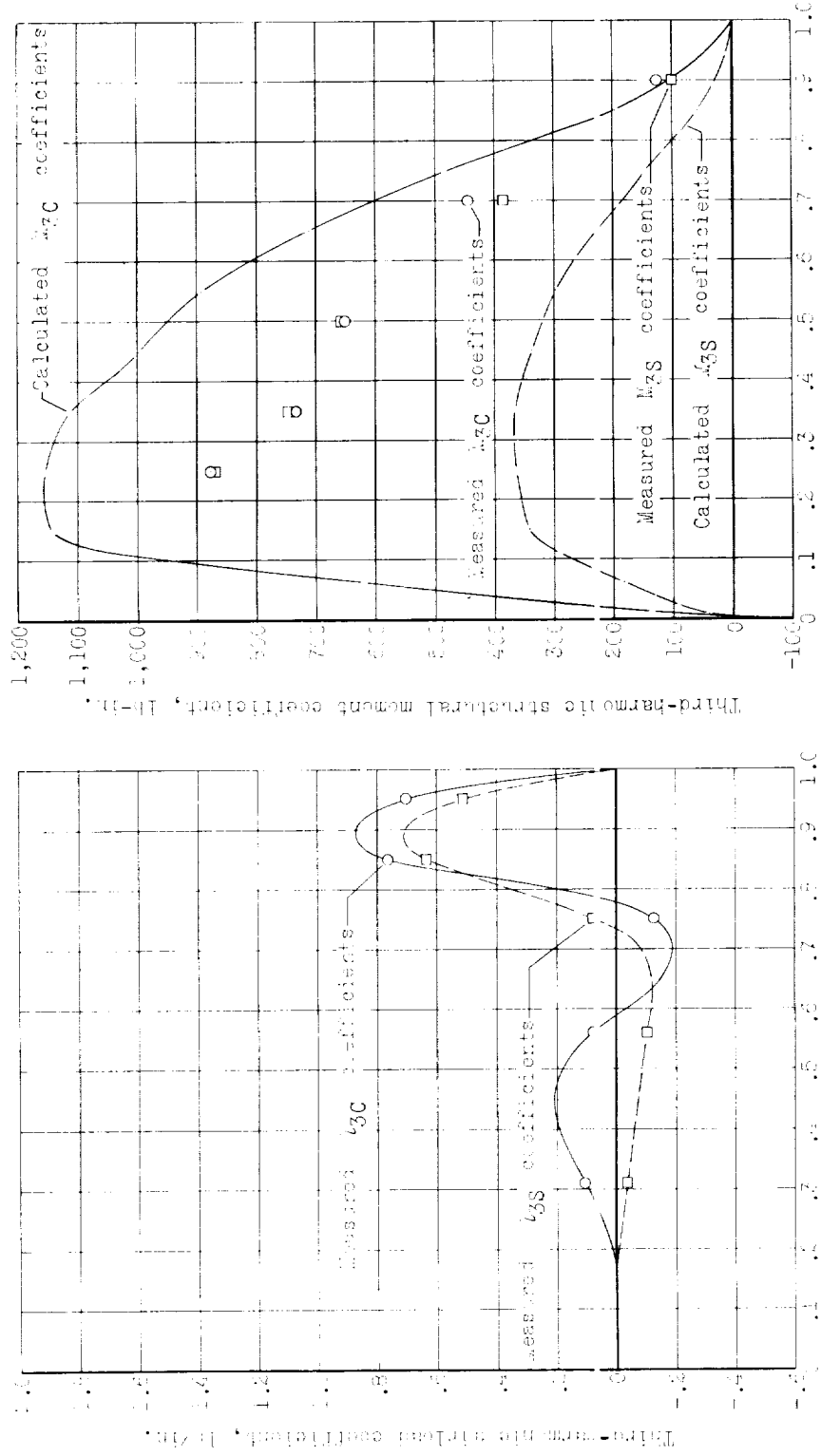

(d) Measured third-harmonic airload coefficients and a comparison of measured and calculated third-harmonic structural moment coefficients.

Figure 10.- Continued.

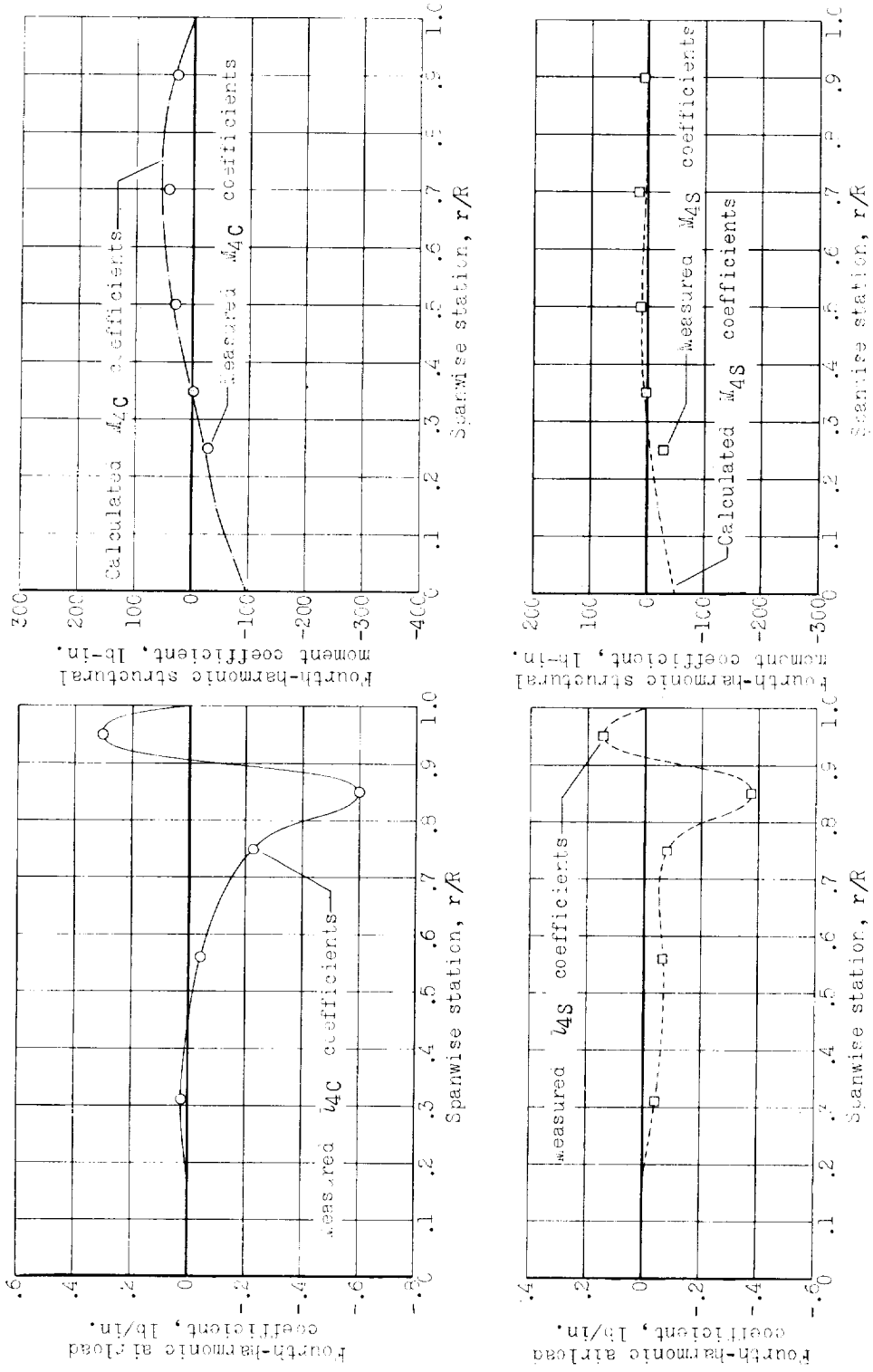

(e) Measured fourth-harmonic airload coefficients and a comparison of measured and calculated fourth-harmonic structural moment coefficients.

Figure 10.- Concluded.

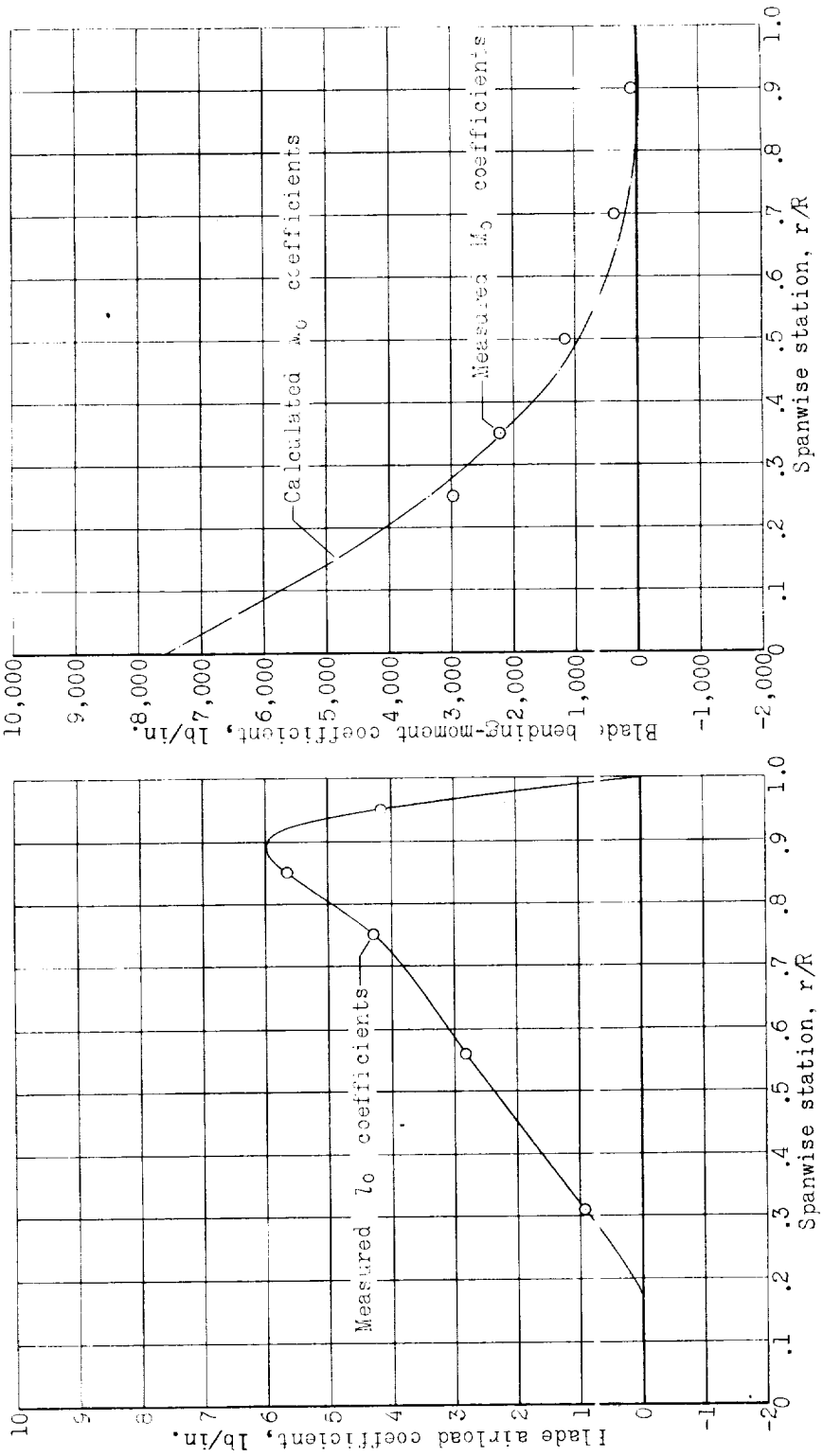

(a) Measured steady airload coefficients and comparison of measured and calculated steady structural moment coefficients.

Figure 11.- Measured airload coefficients and comparison of measured and calculated structural moment coefficients in forward flight. $\mu = 0.15$; airload $C_T = 0.0049$; moment $C_T = 0.0047$.

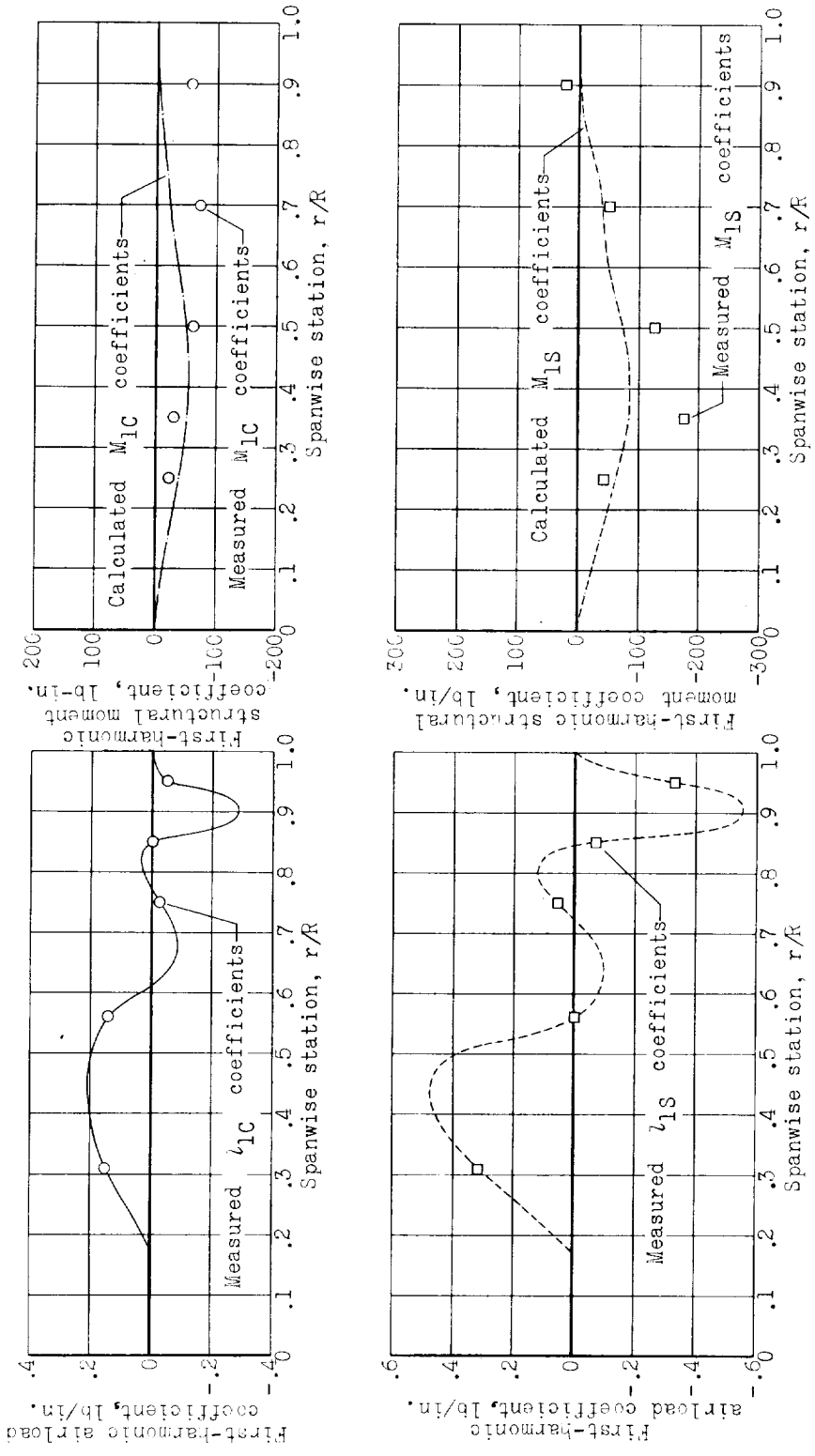

(b) Measured first-harmonic airload coefficients and comparison of measured and calculated first-harmonic structural moment coefficients.

Figure 11.- Continued.

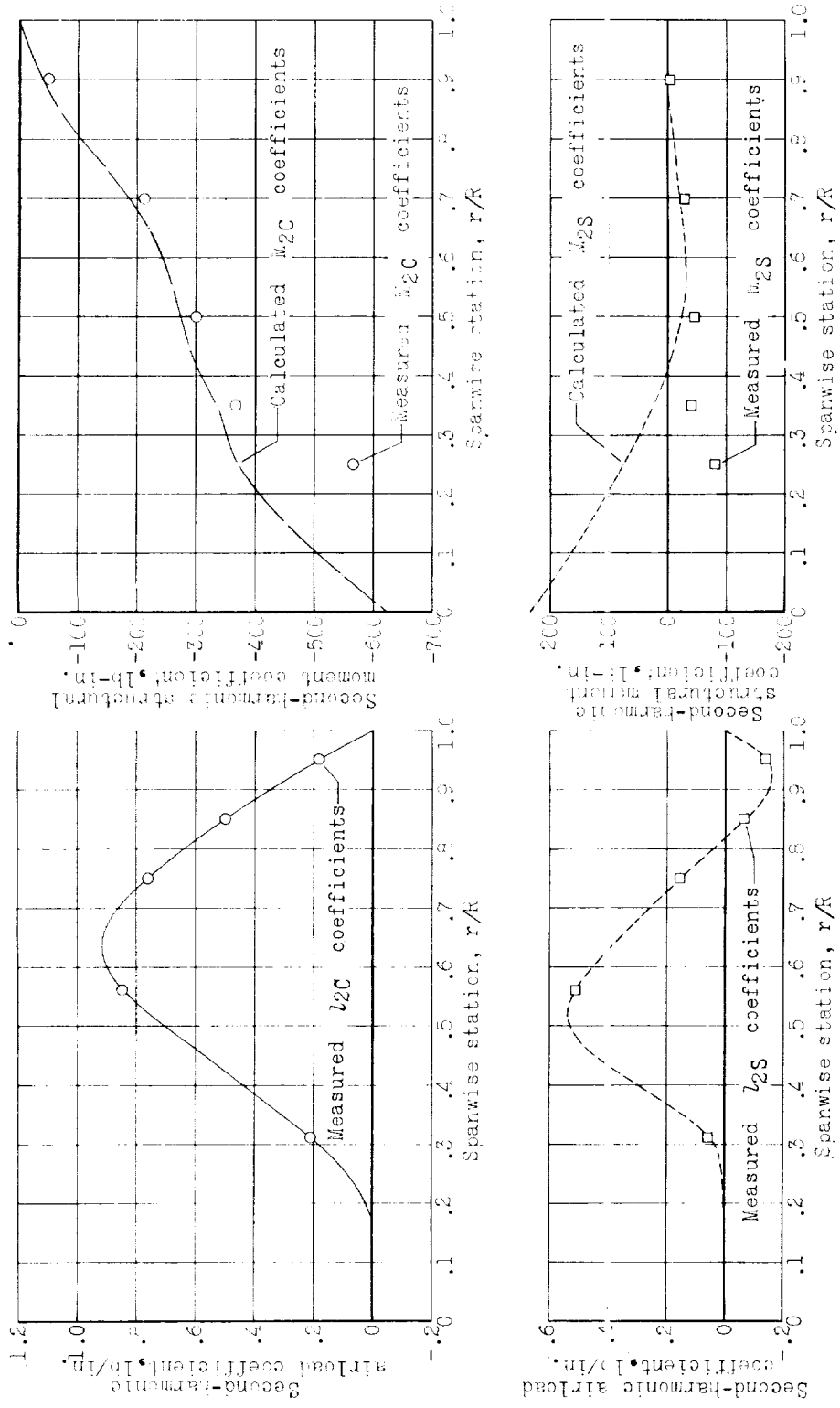

(c) Measured second-harmonic airload coefficients and a comparison of measured and calculated second-harmonic structural moment coefficients.

Figure 11.- Continued.

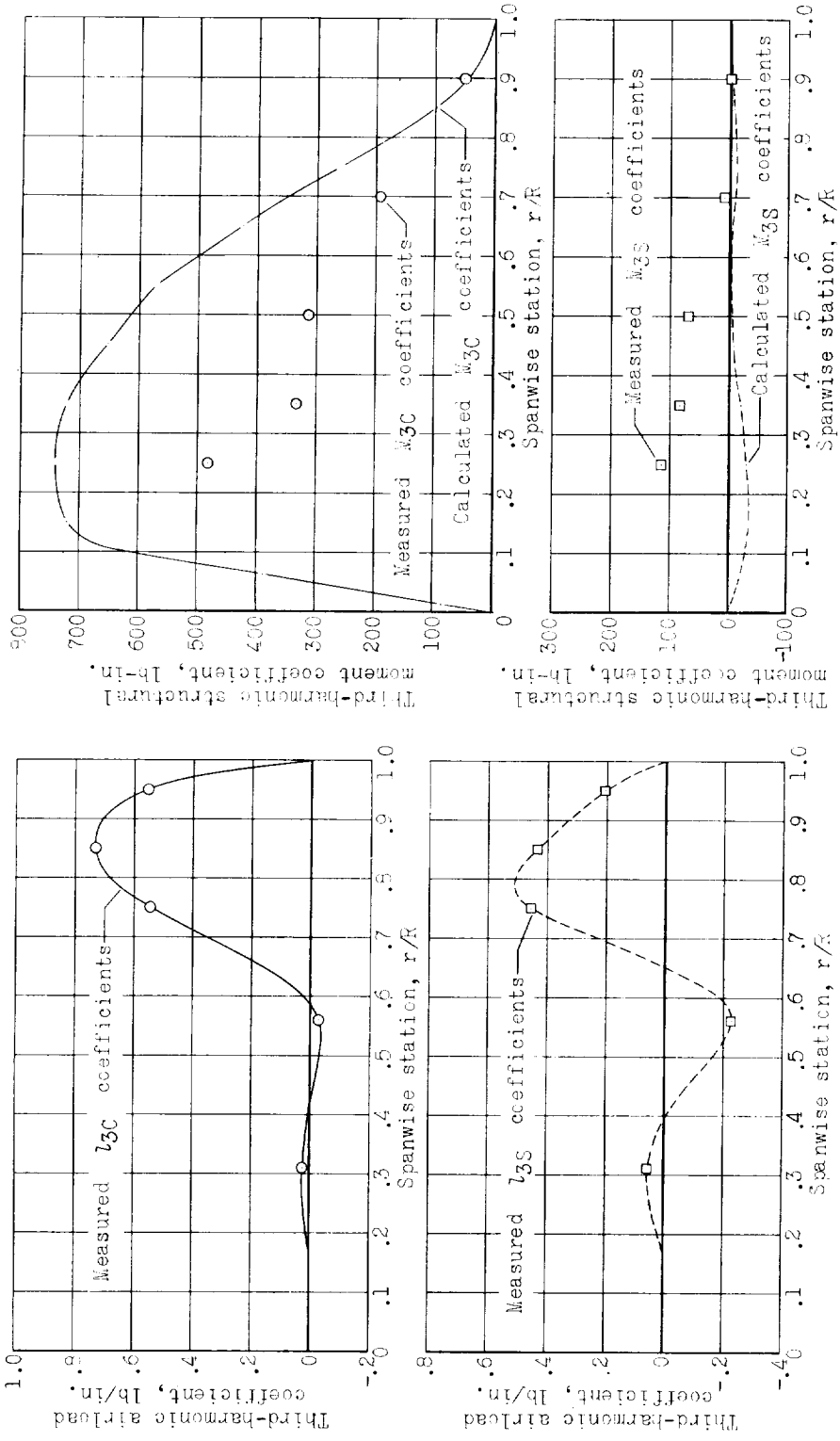

(d) Measured third-harmonic airload coefficients and a comparison of measured and calculated third-harmonic structural moment coefficients.

Figure 11.- Continued.

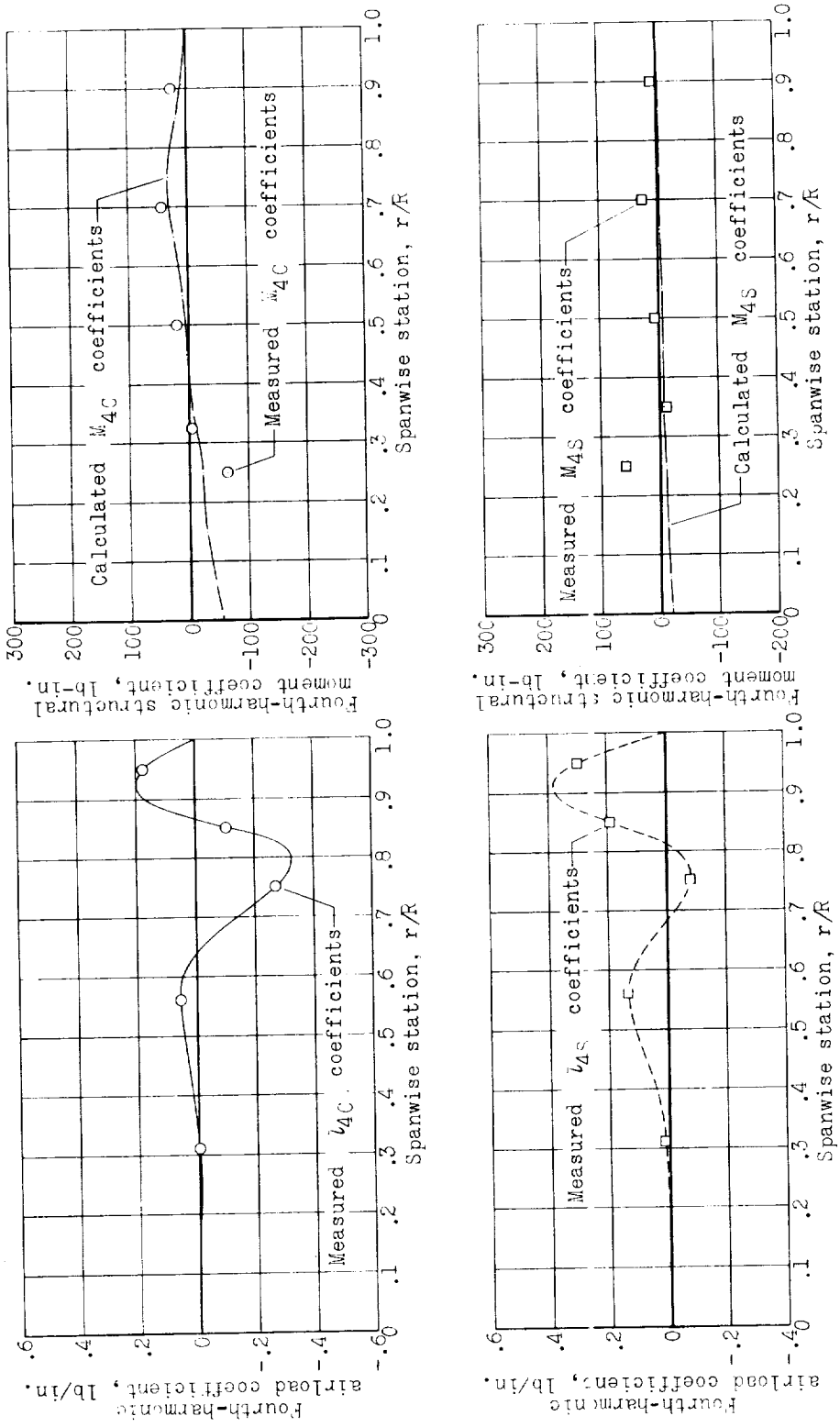

(e) Measured fourth-harmonic airload coefficients and a comparison of measured and calculated fourth-harmonic structural moment coefficients.

Figure 11.- Concluded.

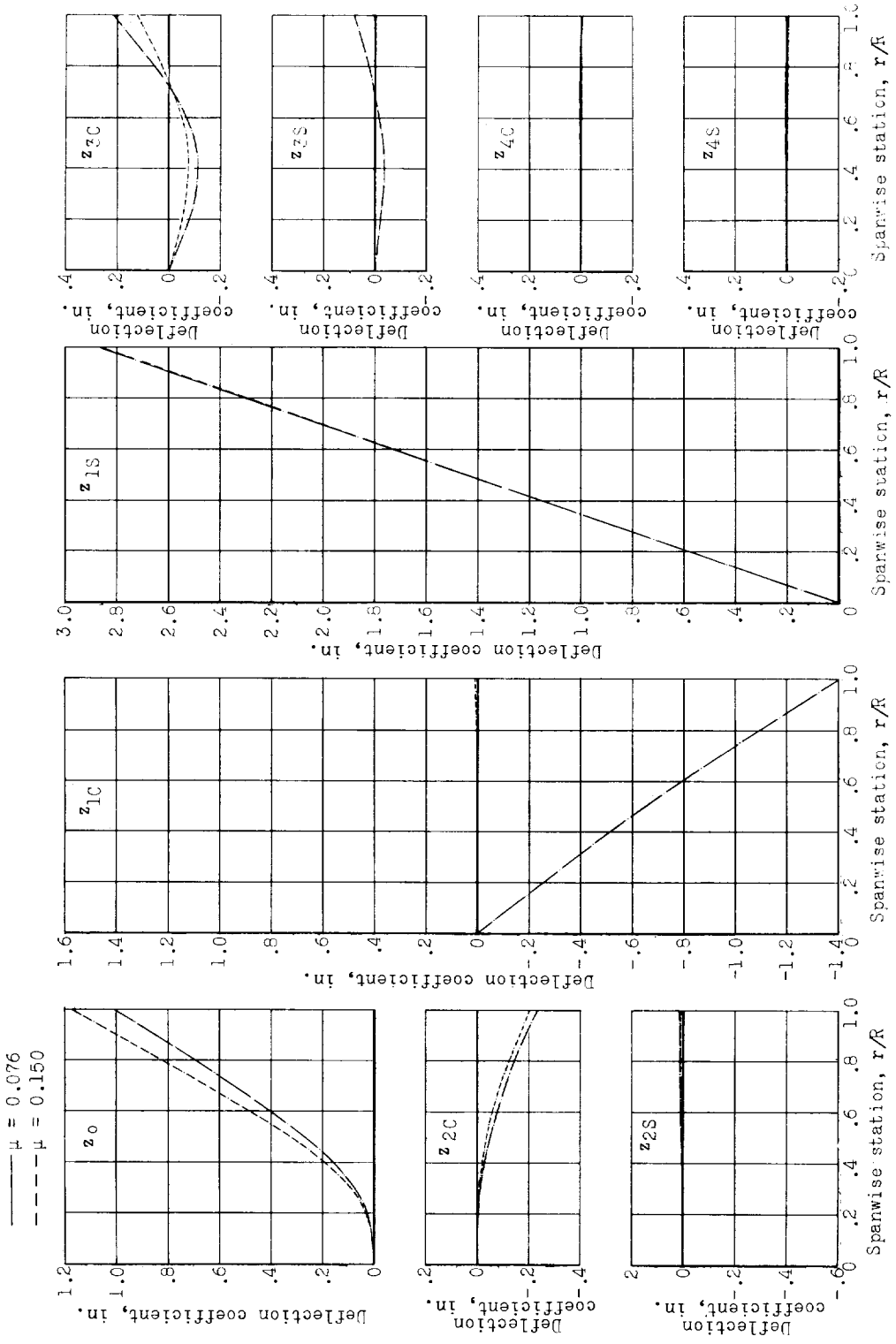

Figure 12.- Calculated blade deflections for the $\mu = 0.076$ and $\mu = 0.15$ forward-flight conditions. $z_{total} = z_o + z_{1c} \cos \psi + z_{1s} \sin \psi + z_{2c} \cos 2\psi + z_{2s} \sin 2\psi + z_{3c} \cos 3\psi + z_{3s} \sin 3\psi + z_{4c} \cos 4\psi + z_{4s} \sin 4\psi$.

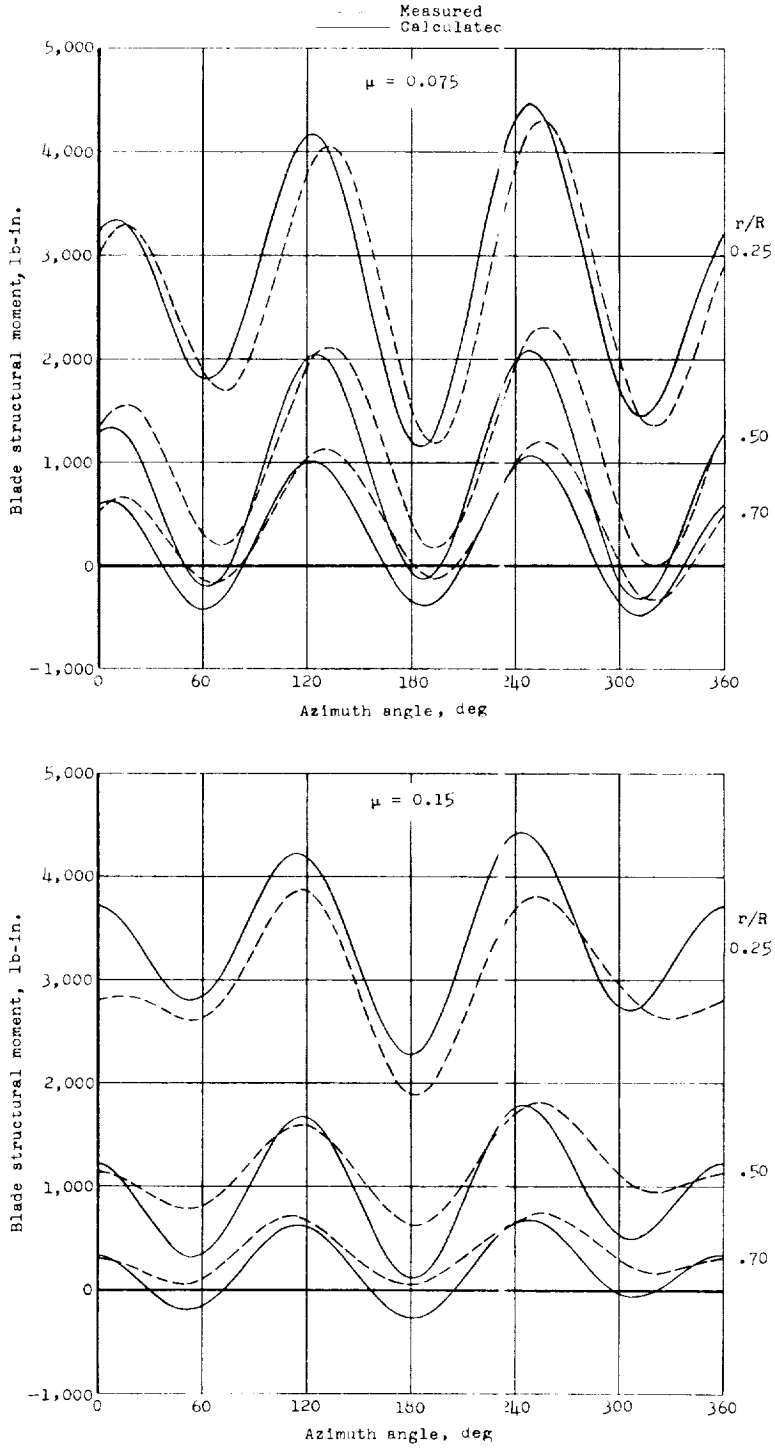

Figure 13.- Comparison of measured and calculated total bending moments.